Hybrid functional calculations of point defects and hydrogen in $SrZrO_3$

L. Weston,[1,2] A. Janotti,[2] X. Y. Cui,[3] C. Stampfl,[1] and C. G. Van de Walle[2]
[1]*School of Physics, The University of Sydney, Sydney, New South Wales 2006, Australia*
[2]*Materials Department, University of California, Santa Barbara, California 93106-5050, USA*
[3]*Australian Centre for Microscopy and Microanalysis, School of Aerospace, Mechanical and Mechatronic Engineering, The University of Sydney, Sydney, New South Wales 2006, Australia*
(Received 31 March 2014; published 22 May 2014)

Using hybrid density functional theory, we investigate the impact of native vacancies and hydrogen impurities on the electrical and optical properties of cubic $SrZrO_3$. Oxygen vacancies (V_O) form localized states and introduce deep donor levels in the gap. The formation energy of V_O is low when the Fermi level is near the valence band; V_O will thus be a compensating center in acceptor-doped $SrZrO_3$. Sr and Zr vacancies (V_{Sr}/V_{Zr}) are acceptor-type defects, and have low formations energies when the Fermi level is near the conduction band. Hole localization on oxygen dangling bonds is an important feature of these vacancies. V_{Sr} is most prevalent and can account for the luminescence peak at 3.4 eV observed in Sr-deficient $SrZrO_3$. Hydrogen impurities are found to preferentially incorporate at an interstitial site (H_i), forming an O-H bond and acting as a donor. H_i can also be stabilized as an acceptor, sitting midway between adjacent Sr atoms; the $\varepsilon(+/-)$ transition level is found at 0.44 eV below the conduction band. Hydrogen can also substitute on an oxygen site (H_O), acting as a shallow donor. The formation energy of H_O is high compared to H_i, yet it is stable with respect to dissociation into H_i and V_O.

DOI: 10.1103/PhysRevB.89.184109 PACS number(s): 61.72.Bb, 61.72.J−, 71.55.Ht

I. INTRODUCTION

Strontium zirconate (SZO), with chemical formula $SrZrO_3$, is a complex oxide with a number of useful properties for device applications. Its features include high-temperature proton conductivity [1], a large dielectric constant [2], resistance switching [3,4], and ferroelectricity in artificial superlattices [5,6]. SZO crystalizes in the perovskite (ABO_3) structure, a class of compounds that is currently of significant research interest due to the emergence of novel interface phenomena [7,8].

Native point defects are known to play an important role in oxides, and in many cases dominate the electronic and optical properties. For example, native defects commonly act as carrier-compensation centers, introduce optically active states in the band gap [9,10], and are sometimes invoked as sources of free carriers [11]. Intentionally and unintentionally incorporated impurities also affect the materials properties; among impurities that can be unintentionally incorporated during growth, hydrogen stands out [12].

Oxygen vacancies (V_O) are donor-type defects, and are commonly invoked as a source or explanation for many defect-related phenomena in oxides. For example, the formation and removal of V_O is thought to be the mechanism behind the resistive switching characteristics of SZO [3]. Oxygen vacancies are also thought to affect device performance: Tang *et al.* [13] found that leakage current in SZO thin-film dielectrics increases with anneal temperature, and the change was attributed to an increase in V_O concentration. However, such assignments are speculative, since to date there have been no direct observations of V_O.

The importance of cation vacancies in SZO is also yet be established; however, first-principles calculations of cation vacancies in $SrTiO_3$ [14] and $BaZrO_3$ [15] suggest that both A- and B-site cation vacancies are acceptors, and can have low formation energies under certain conditions. Results of positron annihilation spectroscopy measurements indicate significant concentrations of cation vacancies in nominally undoped $SrTiO_3$ films [16]. Recently, a broad luminescence peak at 3.39 eV has been observed in Sr-deficient SZO [17]. This signal was attributed to strontium vacancies (V_{Sr}), suggesting that V_{Sr} may form deep-level states in the band gap of SZO.

Impurities may also affect the electronic properties. Hydrogen is known to occupy interstitial sites (H_i) in many oxides. H_i is easily incorporated and can significantly impact the electronic properties of the host material [12,18]. Several lattice sites for H_i have been considered in calculations for perovskite materials (see Fig. 1); for example, in $SrTiO_3$ the positively charged H_i^+ is predicted to form a strong O-H bond, with an H-O-Ti angle of 76° in the (100) plane [19], whereas for $BaZrO_3$, the O-H bond is perpendicular to the Zr-O axis and parallel to the [001] direction [20]. In both cases, H_i forms a strong O–H bond of approximately 1 Å in length. Another study of H_i in $BaZrO_3$ found that the negatively charged H_i^- is repelled by O, and prefers to locate midway between adjacent Ba ions [21]. Hydrogen is also known to substitute at an oxygen site (H_O) in other oxides [22]; in the multicenter-bond configuration, H_O has been reported to act as a shallow donor. Formation of H_O in SZO has not yet been explored.

Drawing concrete conclusions about point defects from experiment can be extremely difficult, and often requires many assumptions. Computational studies of point defects, in particular based on density functional theory (DFT), can provide detailed microscopic information; however, DFT calculations are hindered by the well-known band-gap problem. This can be particularly significant in wide-band-gap materials such as SZO, since the formation energy of defects depends on the position of the Fermi level in the gap. The problem can be overcome, however, by the use of screened hybrid functionals [23], which have been shown to give an accurate description of semiconductor properties including the band gap [24] and defect levels [25,26].

 ©2014 American Physical Society

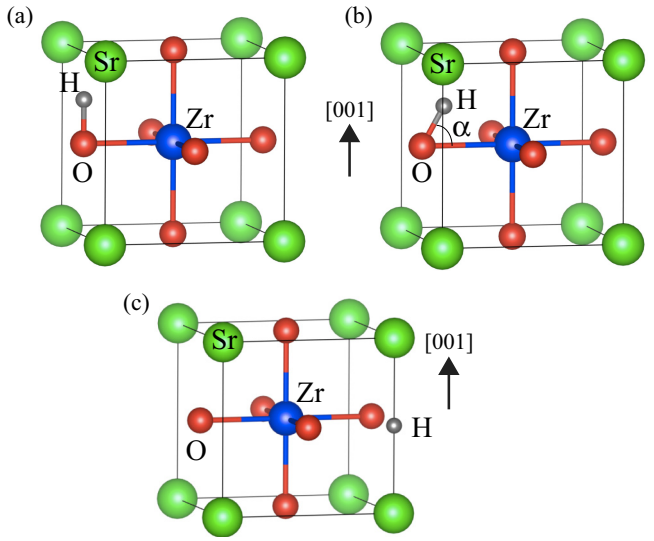

FIG. 1. (Color online) Possible sites occupied by interstitial hydrogen (H_i) in $SrZrO_3$. In (a), the H atom forms an O-H bond perpendicular to the Zr-O axis and parallel to the [001] direction. In (b), the H atom forms an O-H bond at an angle α with the Zr-O bond. In (c), the H atom lies along the line joining two adjacent Sr ions. Sr ions are represented by large (green) spheres at the corner of the cubic primitive cell with Zr (blue) at the center. The O atoms (red) are at the center of the faces. The H atoms are represented by small (dark grey) spheres.

Here we use first-principles calculations based on hybrid density functional theory to investigate the properties of native vacancies (V_{Sr}, V_{Zr}, V_O) and hydrogen impurities (H_i, H_O) in $SrZrO_3$ in the cubic phase. Although the cubic phase is not the ground state at room temperature [27], we expect the defect physics in the *Pbnm* orthorhombic phase to be very close to that in the cubic phase, due to the very similar local environments in the two phases. Moreover, in pseudomorphic structures, epitaxial SZO films assume a pseudocubic structure when grown on cubic substrates [28]. Section II describes the methodology, and Sec. III contains our results and discussion.

II. METHODOLOGY

A. Computational details

Our calculations are performed using DFT with the screened hybrid functional of Heyd, Scuseria, and Ernzerhof (HSE) [23,29]. In this approach, the short-range exchange potential is calculated by mixing a fraction of nonlocal Hartree-Fock exchange with the generalized gradient approximation (GGA) functional of Perdew, Burke, and Ernzerhof (PBE) [30]. The long-range exchange potential and the correlation potential are calculated with the PBE functional. The screening length and mixing parameter are fixed at 10 Å and 0.25 respectively [31,32]. The valence electrons are separated from the core by use of projector-augmented wave (PAW) potentials[33] as implemented in the VASP code [34]. For the present calculations, Sr $4s^2 4p^6 5s^2$, Zr $4d^2 5s^2$, and O $2s^2 2p^4$ electrons are treated as valence. Defects were simulated using a $3 \times 3 \times 3$, 135-atom, cubic supercell, a $2 \times 2 \times 2$ k-point grid for integration over the Brillouin zone, and an energy cutoff of 400 eV for the plane-wave basis set. Spin polarization was taken into account.

B. Defect calculations

For vacancy calculations, one atom is removed from the supercell and the remaining atoms are allowed to relax. The substitutional defect H_O is created by replacing a lattice O by H. For H_i, several configurations are investigated as shown in Fig. 1. First, we consider a site in which the H atom forms an O-H bond perpendicular to the Zr-O bond, oriented along the [001] direction, as in Fig. 1(a). Second, a lower-symmetry site is considered in which the H atom forms an O-H bond at an angle α ($<90^\circ$) with the Zr-O bond, with the H, O, and Zr atoms residing in the same (100) plane, as shown in Fig. 1(b). A final site is considered in which the H atom is located along the line joining two adjacent Sr ions [Fig. 1(c)].

For a defect D_i in charge state q, the formation energy $E^f[D_i^q]$ is calculated as [35]

$$E^f\left[D_i^q\right] = E_{\text{tot}}\left[D_i^q\right] - E_{\text{tot}}[\text{SZO}] + \mu_i + qE_F + \Delta^q, \tag{1}$$

where $E_{\text{tot}}[D_i^q]$ is the total energy of the supercell containing D_i^q, and $E_{\text{tot}}[\text{SZO}]$ is the total energy of the defect-free supercell. The chemical potential μ_i represents the energy associated with the reservoir with which atoms are exchanged; μ_{Sr} is referenced to the total energy per atom of bulk Sr in the fcc crystal structure, μ_{Zr} to that of bulk Zr in the hcp structure, and μ_O is referenced to half of the total energy of an O_2 molecule. The electron chemical potential is given by the position of the Fermi level (E_F), taken with respect to the valence-band maximum (VBM) E_v. Finally, the term Δ^q is the charge-state dependent correction due to the finite size of the supercell [36,37].

The defect charge-state transition level $\varepsilon(q/q')$ is defined as the Fermi level position below which the defect is stable in the charge state q, and above which it is stable in charge state q'. It is calculated as

$$\varepsilon(q/q') = \frac{E^f\left(D_i^q; E_F = 0\right) - E^f\left(D_i^{q'}; E_F = 0\right)}{q' - q}, \tag{2}$$

where $E^f(D_i^q; E_F = 0)$ is the formation energy of D_i^q when the Fermi level is at the VBM (i.e, for $E_F = 0$).

C. Chemical potentials

Equation (1) shows that defect formation energies depend on the chemical potential of the associated atomic species. The chemical potential can be related to experimental conditions during growth or processing, such as temperature and pressure, and this quantity is a variable in the formalism [35]. However, bounds are placed on these values by imposing the conditions for stability of SZO in thermodynamic equilibrium:

$$\mu_{Sr} + \mu_{Zr} + 3\mu_O = \Delta H_f(SrZrO_3). \tag{3}$$

In order to prevent formation of bulk Sr and Zr phases, and to prevent loss of O_2, the chemical potentials are bounded from above by

$$\mu_{Sr}, \mu_{Zr}, \mu_O \leqslant 0. \tag{4}$$

To prevent formation of secondary SrO and ZrO_2 phases, it is required that

$$\mu_{Sr} + \mu_O \leqslant \Delta H_f(SrO), \quad (5)$$

$$\mu_{Zr} + 2\mu_O \leqslant \Delta H_f(ZrO_2). \quad (6)$$

The quantities $\Delta H_f(SrZrO_3)$, $\Delta H_f(SrO)$, and $\Delta H_f(ZrO_2)$ are the enthalpies of formation of SrO, ZrO_2, and $SrZrO_3$, respectively, and these are calculated from first principles. Combining Eqs. (3) and (5) gives

$$\mu_{Zr} + 2\mu_O \geqslant \Delta H_f(SrZrO_3) - \Delta H_f(SrO). \quad (7)$$

The inequalities in Eqs. (6) and (7) allow us to describe the region of chemical potentials in the μ_{Zr}-μ_O plane for which SZO is stable.

III. RESULTS AND DISCUSSION

A. Bulk properties

We first present the results for the structural and electronic properties of defect-free bulk cubic SZO. The calculated lattice parameter and band gap for cubic SZO are listed in Table I. The calculated lattice parameter is 4.175 Å, which is within 0.5% of the experimental value of 4.154 Å [27].

The calculated electronic band structure of cubic SZO is shown in Fig. 2. The uppermost valence band is composed mainly of O $2p$ orbitals. The VBM is located at the R point, 0.34 eV higher in energy than at Γ. The lower conduction-band states are composed mostly of Zr $4d$ orbitals, with the conduction-band minimum (CBM) occurring at Γ. The octahedral crystal field splits the degeneracy of the Zr $4d$ states; the lowest conduction bands originate from the t_{2g} orbitals. The e_g-derived bands are 4.2 eV higher in energy.

The calculated indirect gap (R–Γ) is 4.70 eV, and the direct gap at Γ is 5.04 eV. These HSE values are in reasonable agreement with B3LYP calculations by Sambrano *et al.* [39], who reported indirect and direct gaps of 4.86 and 5.07 eV, respectively. The band gap of the cubic phase has not been measured experimentally. For the orthorhombic phase, the reported band-gap values lie in the range of 5.2–5.6 eV [40,41]. Our calculated direct band gap (at Γ) for the orthorhombic phase is 5.16 eV, close to the result of Zhang *et al.* [40], who measured a band gap of 5.2 eV based on the absorption edge.

TABLE I. Calculated equilibrium lattice parameter, as well as direct (Γ–Γ) and indirect (R–Γ) band gaps for $SrZrO_3$ in the cubic phase. Results from previous calculations and experiments are listed for comparison.

			Band gap (eV)	
		a (Å)	Γ–Γ	R–Γ
Present	HSE	4.175	5.04	4.70
Other DFT	PBE[a]	4.196	3.50	3.23
	B3LYP[b]	4.144	5.07	4.86
Experiment		4.154[c]	5.2–5.6[d]	

[a]Reference [38].
[b]Reference [39].
[c]Reference [27].
[d]References [40,41], for orthorhombic SZO.

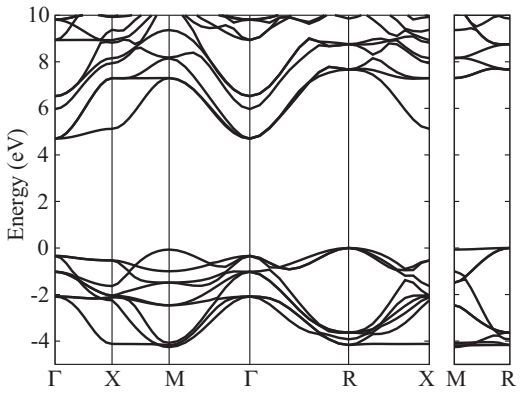

FIG. 2. Bulk band structure of cubic $SrZrO_3$, calculated along the high-symmetry path in the Brillouin zone. The zero of energy is set at the VBM (at the R point). The indirect band gap (R–Γ) is calculated to be 4.70 eV.

The fact that the orthorhombic phase has a band gap larger than the cubic phase is not unexpected, since the orthorhombic distortion should widen the band gap [42,43].

B. Point defects in $SrZrO_3$

The region of chemical potential in the μ_{Zr}-μ_O plane for which SZO is stable is illustrated in Fig. 3. The boundaries of this region are defined by the following enthalpies of formation, which have been calculated with the HSE functional: $\Delta H_f(SrO) = -5.63$ eV, $\Delta H_f(ZrO_2) = -10.77$ eV, and $\Delta H_f(SrZrO_3) = -16.85$ eV. The upper (blue) line is given by Eq. (6), and the lower (red) line is given by Eq. (7). Combinations of μ_{Zr} and μ_O which fall between the two boundaries lead to stable SZO; the corresponding μ_{Sr} can be extracted from Eq. (3).

Within the SZO stability region, the oxygen chemical potential can in principle vary over the wide range of

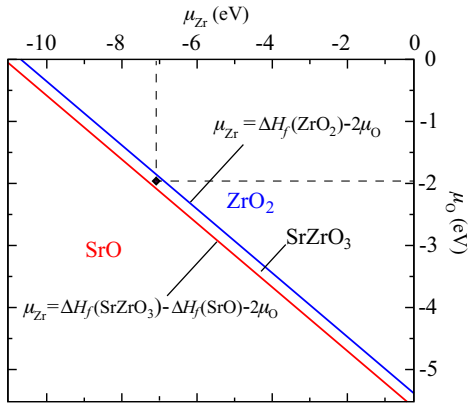

FIG. 3. (Color online) Chemical stability region for $SrZrO_3$ in the μ_{Zr}-μ_O plane. Combinations of μ_{Zr} and μ_O below the lower (red) line lead to precipitation of SrO, and in the region above the upper (blue) line to precipitation of ZrO_2. The region between the two lines corresponds to chemical potentials for which $SrZrO_3$ is stable. The value of $\mu_O = -1.94$ eV, representing growth conditions [44], and the corresponding μ_{Zr} used to determine defect formation energies are indicated.

TABLE II. The formation energy (E^f) of defects in $SrZrO_3$ in different charge states, taking $\mu_O = 0$ eV, $\mu_{Zr} = -11.00$ eV, $\mu_{Sr} = -5.86$ eV, and $\mu_H = -1.34$ eV. The Fermi level was set at the VBM ($E_F = 0$ eV).

Defect	Charge state	$E^f(E_F = 0)$ eV
V_O	0	4.97
	+1	0.80
	+2	−2.33
V_{Sr}	0	2.85
	−1	3.11
	−2	4.05
V_{Zr}	0	7.36
	−1	5.63
	−2	8.81
	−3	9.49
	−4	10.30
H_i	+1	−3.36
	0	1.30
	1−	5.18
H_O	+	1.16

$-5.61 \leqslant \mu_O \leqslant 0$ eV. In Table II, we list defect formation energies for $\mu_O = 0$ eV and Fermi level at the VBM; The Zr chemical potential was set to $\mu_{Zr} = -11.00$ eV, i.e., between the limits set by Eqs. (6) and (7), for simplicity, and $\mu_{Sr} = -5.86$ eV was obtained from Eq. (3). For the hydrogen impurity, there exists an upper bound on μ_H to avoid formation of H_2O, $2\mu_H + \mu_O \leqslant \Delta H_f(H_2O)$. Our calculated HSE value for the formation enthalpy of H_2O is $\Delta H_f(H_2O) = -2.68$ eV (at $T = 0$), in good agreement with the experimental value (–2.56 eV) [45], and so we set $\mu_H = -1.34$ eV for $\mu_O = 0$ eV. We note formation energies for different sets of chemical potentials, representing growth conditions, can be obtained using Eq. (1) and the values listed in Table II.

In the following we discuss the results of formation energies for a set of chemical potentials that represent growth by pulsed laser deposition ($T = 1200$ K, $p_{O_2} = 5 \times 10^{-6}$ bar [44]), corresponding to $\mu_O = -1.94$ eV. For μ_{Zr} we take the midpoint of the allowed range, i.e., $\mu_{Zr} = -7.11$ eV, resulting in $\mu_{Sr} = -3.92$ eV. For H-related defects, we consider a background partial pressure of $p_{H_2} = 10^{-8}$ bar at 1200 K, which corresponds to $\mu_H = -1.70$ eV.

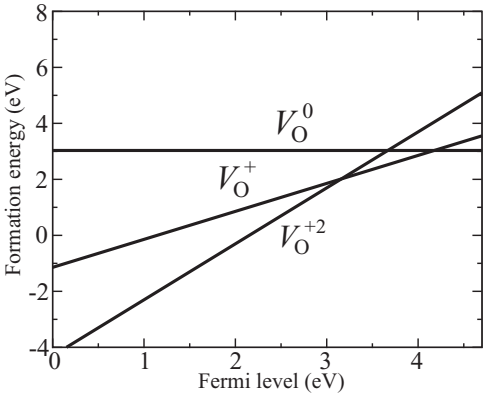

FIG. 5. Formation energy of the oxygen vacancy as a function of the Fermi level for the neutral (V_O^0), positive (V_O^+), and 2+ (V_O^{2+}) charge states. The points where lines intersect correspond to charge-state transition levels [Eq. (2)]. Results are shown for $\mu_O = -1.94$ eV, representing growth conditions as described in the text.

1. Oxygen vacancies

The O atom in SZO is twofold coordinated, bonded to two Zr atoms. Removing an O atom leaves two Zr dangling bonds with d-orbital character, which then form a bonding state at an energy 1.26 eV below the CBM, and an antibonding state resonant in the conduction band. In the neutral charge state, V_O^0, the bonding state is doubly occupied. The charge density of this gap state is shown in Fig. 4(a). The two Zr atoms are displaced towards the vacant site by 0.22 Å. In the positive charge state, V_O^+, the Zr atoms are displaced slightly towards the vacancy, by 0.04 Å, and the spin-up single-particle state in the gap is located at 1.83 eV below the CBM. The unoccupied spin-down state is above the CBM. Finally, in the doubly positive charge state, V_O^{+2}, the two Zr atoms are displaced slightly away from the vacancy (by 0.002 Å), and the unoccupied vacancy states are both resonant in the conduction band.

Formation energies of V_O in its various charge states are shown in Fig. 5. The charge-state transition levels of V_O, determined from Eq. (2), are represented by the intersection

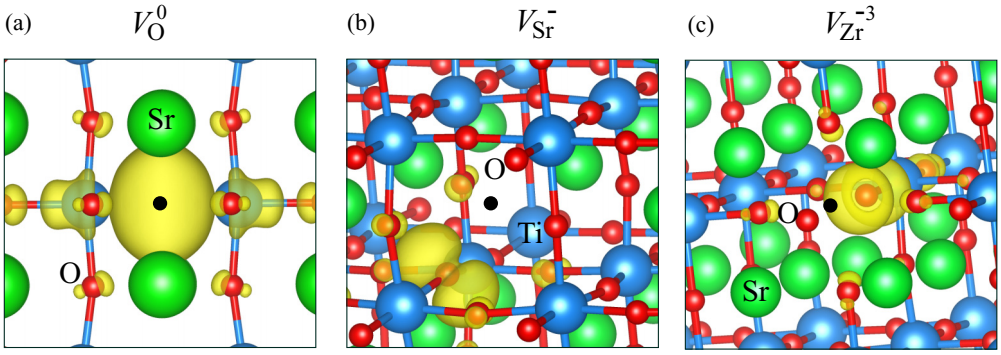

FIG. 4. (Color online) (a) Charge density isosurface for the gap state of the neutral oxygen vacancy V_O^0 in $SrZrO_3$; (b) spin density isosurface for the Sr vacancy, V_{Sr}^-; (c) spin density isosurface for the Zr vacancy, V_{Zr}^{-3}. The isosurfaces (yellow) correspond to 10% of the maximum density value.

of the formation-energy lines. The calculated values are $\varepsilon(+2/+) = 3.13$ eV (1.57 eV below the CBM) and $\varepsilon(+/0) = 4.17$ eV (0.53 eV below the CBM), indicating that V_O is a deep donor in SZO.

The formation energy of V_O decreases as the Fermi level approaches the valence band, indicating that this defect is a major compensating center in acceptor-doped SZO, as would be the case in yttrium-doped SZO for fuel cells [1]. On the other hand, the formation energy of V_O increases when the Fermi level approaches the conduction band; combined with its deep-donor character, this indicates that V_O does not cause n-type conductivity in SZO.

2. Strontium vacancies

Sr atoms in the cubic perovskite lattice are 12-fold coordinated by nearest-neighbor O atoms. Removal of a Sr atom from the SZO lattice, while keeping the lattice unrelaxed, leaves two holes in the valence band, indicating that V_{Sr} will act as a double acceptor. By slightly perturbing the atomic positions around the vacancy, and allowing the atoms to relax, we observe that the holes become localized on individual O atoms neighboring the vacancy, reducing the local cubic symmetry. The broken-symmetry configuration, in which the two holes are localized, is lower in energy by 1.1 eV than the configuration in which the O atoms are relaxed symmetrically around the vacancy. In the case of the negatively charged vacancy V_{Sr}^{-1}, the single hole is localized on one of the O atoms; this configuration is lower by 0.9 eV than a symmetric configuration.

The formation energies of V_{Sr} in the neutral, -1, and -2 charge states as a function of E_F are shown in Fig. 6. The acceptor transition levels are at $\varepsilon(0/-) = 0.3$ eV and $\varepsilon(-/-2) = 0.9$ eV, indicating that V_{Sr} is a deep acceptor. V_{Sr} is most stable in the -2 charge state, except for Fermi levels within 0.9 eV of the VBM; such low values of E_F are unlikely to occur experimentally. The formation energy of V_{Sr}^{-2} decreases with increasing E_F across the gap, indicating that V_{Sr} is a likely source of donor compensation.

The spin density for V_{Sr}^{-1}, which roughly corresponds to the charge density of the unpaired electron at the vacancy, is plotted in Fig. 4(b). The O atom with the unpaired electron is displaced towards the vacancy by 0.90 Å, giving rise to a

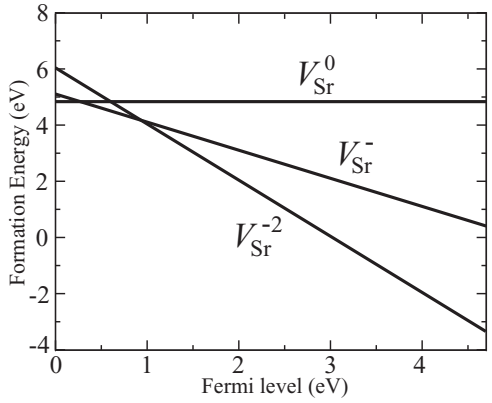

FIG. 6. Formation energy of the strontium vacancy (V_{Sr}) as a function of the Fermi level for the neutral (V_{Sr}^0), negative (V_{Sr}^-), and -2 (V_{Sr}^{-2}) charge states. The points where lines intersect correspond to charge-state transition levels. Results are shown for $\mu_{Sr} = -3.92$ eV.

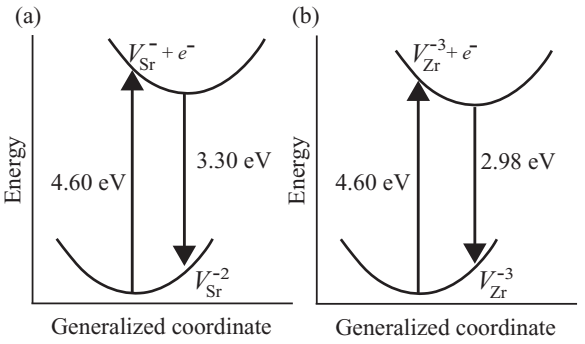

FIG. 7. Configuration coordinate diagram for excitation and emission energies associated with (a) V_{Sr} and (b) V_{Zr}. In (a) an electron is excited from V_{Sr}^{-2} to the CBM; the electron recombines with the hole at V_{Sr}^{-}. In (b) an electron is excited from V_{Zr}^{-4} to the CBM; the electron recombines with the hole at V_{Zr}^{-3}.

localized state in the gap and resulting in an $S = 1/2$ center. Similarly, at V_{Sr}^0 there are two unpaired electrons localized on opposing O atoms with total spin $S = 1$. We note that these are paramagnetic centers that could in principle be observed by electron paramagnetic resonance (EPR). Since the -1 and neutral charge states are thermodynamically stable only when the Fermi level is close to the VBM, which is experimentally unlikely to occur, optical excitation would be required to create the paramagnetic states. In the case of V_{Sr}^{-2}, there are no gap states and the neighboring O atoms relax symmetrically away from the vacancy.

Since V_{Sr} induces levels in the gap, we expect it to lead to deep-level luminescence. We assume that V_{Sr} is initially in the -2 charge state. The defect can be excited in two ways: first, by lifting an electron out of the defect state into the CB, corresponding to the process $V_{Sr}^{-2} \rightarrow V_{Sr}^{-1} + e^-$, where e^- represents an electron at the CBM, and taking V_{Sr}^{-1} in the same atomic arrangement as V_{Sr}^{-2}; this results in a calculated absorption peak of 4.6 eV. The second possibility is excitation with above-band-gap light, which creates electron-hole pairs. A hole can be trapped by the vacancy, again resulting in V_{Sr}^{-1} with an unoccupied defect state in the gap. Whatever the excitation mechanism, an excited electron in the conduction band can then recombine with the hole at V_{Sr}^{-1}, emitting a photon. The emission peak can be calculated by considering the process $V_{Sr}^{-1} + e^- \rightarrow V_{Sr}^{-2}$, taking V_{Sr}^{-2} in the same atomic arrangement as V_{Sr}^{-1}. The calculated emission energy is 3.3 eV, i.e., the Stokes shift is 1.3 eV, as shown in Fig. 7(a). This calculated emission energy is in very good agreement with a luminescence peak at 3.40 eV recently reported in Sr-deficient SZO [17]. The experimental absorption energy from the excitation spectrum was 4.58 eV, also in good agreement with the calculation. We note, however, that these experiments were performed for SZO in the *Pbnm* structure, while the calculations were performed for the cubic phase. Our calculated emission and absorption peaks would be slightly larger if calculations were to be performed for the orthorhombic structure.

3. Zirconium vacancies

In SZO, each Zr is bonded to six O atoms, in an octahedral configuration. Removal of a Zr from the crystal leaves oxygen

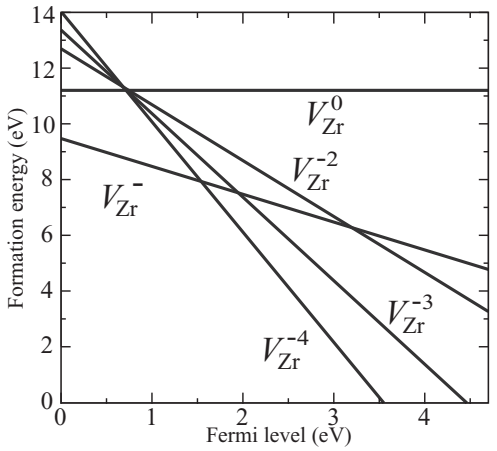

FIG. 8. Formation energy of the zirconium vacancy (V_{Zr}) as a function of the Fermi level for the neutral (V_{Zr}^{0}) and negative (V_{Zr}^{-}, V_{Zr}^{-2}, V_{Zr}^{3-}, V_{Zr}^{4-}) charge states. The points where lines intersect correspond to charge-state transition levels. Results are shown for $\mu_{Zr} = -7.11$ eV, representing growth conditions.

dangling bonds that, combined, can accept up to four electrons. We observe it is energetically more favorable for each of the four holes to be localized at individual O atoms; in our calculations for V_{Zr}^{0}, when symmetry breaking is allowed, four neighboring oxygens move closer to the vacancy by 0.04 Å. In a similar fashion, the charge states V_{Zr}^{-1}, V_{Zr}^{-2}, and V_{Zr}^{-3} hold three, two, or one holes, respectively, and a corresponding number of neighboring oxygens relax inwards. As an example, the spin density for V_{Zr}^{-3}, which is approximately equal to the charge density for the unpaired electron at the vacancy, is plotted in Fig. 4(c), showing localization on a single O atom.

The formation energy of V_{Zr} in different charge states as a function of E_F is shown in Fig. 8. $E^f[V_{Zr}]$ decreases with increasing E_F position in the gap. The $\varepsilon(0/-)$ transition is inside the valence band, and therefore the neutral charge state is not stable. We find the $\varepsilon(-/-4)$ transition level at 1.6 eV; the -2 and -3 charge states are not thermodynamically stable, either.

A comparison of Figs. 6 and 8 shows that the formation energy of V_{Zr} is always higher than that of V_{Sr}, unless E_F is higher than 4.1 eV. Considering that the chemical potentials μ_{Sr} and μ_{Zr} only vary by 0.45 eV between the Zr-rich and Sr-rich limits, it can be concluded that V_{Sr} is the most prevalent cation vacancy. Since SZO is an insulator, we expect that in the absence of impurities the Fermi-level position will be determined by equivalent concentrations of acceptors and donors. In this case, the Fermi level would be located at 2.6 eV, where the formation energy of V_{Sr}^{-2} is equal to that of V_{O}^{+2}.

We also considered the possibility of V_{Zr} acting as a luminescence center. Under optical excitation, a hole becomes trapped at V_{Zr} state; an electron in the conduction band then recombines with the hole trapped at V_{Zr}^{-3} [Fig. 4(c)]. The predicted peak of the optical emission occurs at 2.98 eV, as shown in Fig. 7(b).

C. Hydrogen impurities

For interstitial hydrogen in the positive and neutral charge states, we find that the H atom forms a strong O-H bond at an angle $\alpha < 90^\circ$ with the O-Zr bond, as shown in Fig. 1(b). H_i^+

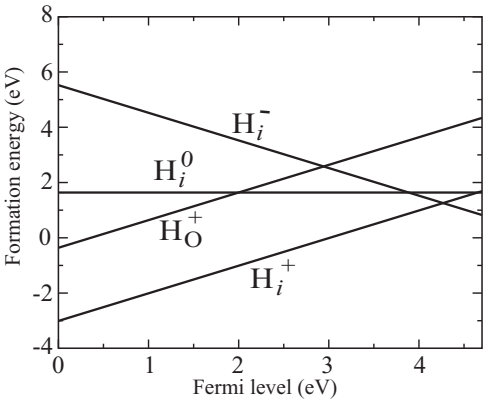

FIG. 9. Formation energy of hydrogen impurities as a function of the Fermi level for interstitial (H_i) and substitutional (H_O) configurations. Results are shown for $\mu_H = -1.70$ eV and $\mu_0 = -1.94$ eV.

forms an O-H bond of length 0.99 Å and at an angle $\alpha = 78^\circ$. We find that the site with $\alpha = 90^\circ$ [at which O-H and O-Zr are perpendicular, see Fig. 1(a)] is unstable and the H atom spontaneously relaxes to its ground-state configuration. In this configuration H lies in the (100) plane; starting configurations with H displaced out of this plane always relax back to the higher-symmetry configuration of Fig. 1(b). In the negative charge state, H_i^- prefers the site along the line joining two adjacent Sr ions, equidistant from them, as shown in Fig. 1(c).

The formation energy of H_i is plotted as a function of E_F in Fig. 9. H_i is stable in the positive charge state for most Fermi-level positions; only when E_F approaches the CBM does H_i^- become more stable, with the $\varepsilon(+/-)$ transition located at 4.26 eV. This result is in agreement with calculations using the weighted density approximation (WDA) [46], where a transition $\varepsilon(+/-) = 4.3$ eV was reported for H_i in SZO.

We also investigate substitutional hydrogen. For hydrogen substituting on an oxygen site (H_O) we find a multicenter-bond configuration [22], in which H sits at the O site and stays equally distant from its two nearest neighbor Zr atoms. The formation energy of H_O is shown in Fig. 9. Interestingly, the $+1$ charge state is stable over the entire range of E_F, indicating that H_O acts as a shallow donor in SZO. Achieving actual n-type doping would probably not be possible, of course, due to the low formation energy of compensating acceptors such as Sr and Zr vacancies. Inspection of the band structure shows that H_O forms a bonding state (between the H $1s$ state and the gap state of V_O^0) located at 4.01 eV below the VBM, indicating strong bonding. The corresponding antibonding state is resonant with the conduction band; the extra electron introduced by H occupies the lowest available energy state at the CBM, making H_O a shallow donor in SZO, as in a number of other oxides [22].

Since the formation of H_O involves removal of a substitutional O atom, the formation energy $E^f[H_O]$ depends on μ_O. For the growth conditions assumed here ($\mu_O = -1.94$ eV and $\mu_H = -1.70$ eV), $E^f[H_O{}^+]$ is 2.6 eV higher than $E^f[H_i{}^+]$. Still, H_O is stable with respect to dissociation into H_i and V_O. The binding energy of H_O^+, calculated as $E^b[H_O^+] = E^f[H_i^+] + E^f[V_O^0] - E^f[H_O^+]$, is 0.45 eV. We note that H_O is more likely to form during growth, as V_O^{+2} and H_i^+, which

are the stable charge states of the O vacancy and interstitial H, would repel each other.

IV. SUMMARY

Using the HSE hybrid functional, we have investigated the role of native vacancies and the hydrogen impurity in cubic $SrZrO_3$. We find that V_O is a deep double donor, and likely to compensate acceptors such as in yttrium-doped SZO used in fuel cells. Cation vacancies are acceptor defects. When holes are generated under optical excitation, hole localization occurs on oxygen atoms neighboring the vacancy, significantly affecting formation and transition energies. The oxygen atom on which the hole is localized relaxes inwards towards the vacancy, resulting in a reduced-symmetry configuration. The resulting paramagnetic states could be observed by EPR under light excitation.

Our results show that V_{Sr} has a lower formation energy than V_{Zr}; we conclude that among cation vacancies V_{Sr} will dominate under typical growth conditions. Our calculations reveal that radiative recombination at V_{Sr} produces a luminescence peak at 3.3 eV, close to the signal at 3.40 eV recently observed in Sr-deficient SZO [17] and thus explaining the origin of this optical emission.

For hydrogen we find that the interstitial is stable in the +1 charge state for most of the range of E_F, and prefers to occupy an off-axis site. Substitutional H_O is a shallow donor, forming a multicenter bond. The formation energy of this defect is higher than that of H_i, but with a binding energy of 0.45 eV with respect to dissociation into H_i^+ and V_O^0.

ACKNOWLEDGMENTS

This work was supported by the NSF MRSEC Program (DMR-1121053). L.W. was supported by the International Center for Materials Research (ICMR), an NSF-IMI Program (DMR08-43934). L.W., X.Y.C., and C.S. also acknowledge support from the Australian Research Council. Computational resources were provided by the Center for Scientific Computing at the CNSI and MRL (an NSF MRSEC, DMR-1121053) (NSF CNS-0960316), and by the Extreme Science and Engineering Discovery Environment (XSEDE), supported by the NSF (OCI-1053575 and DMR07-0072N).

[1] T. Yajima, H. Suzuki, T. Yogo, and H. Iwahara, Solid State Ionics **51**, 101 (1992).
[2] X. Lu, G. Shi, J. Webb, and Z. Liu, Appl. Phys. A **77**, 481 (2003).
[3] M.-H. Lin, M.-C. Wu, C.-Y. Huang, C.-H. Lin, and T.-Y. Tseng, J. Phys. D: Appl. Phys. **43**, 295404 (2010).
[4] C.-C. Lin, B.-C. Tu, C.-C. Lin, C.-H. Lin, and T.-Y. Tseng, IEEE Electron Device Lett. **27**, 725 (2006).
[5] T. Tsurumi, T. Harigai, D. Tanaka, S. Nam, H. Kakemoto, S. Wada, and K. Saito, Appl. Phys. Lett. **85**, 5016 (2004).
[6] T. Harigai, S. Nam, H. Kakemoto, S. Wada, K. Saito, and T. Tsurumi, Thin Solid Films **509**, 13 (2006).
[7] H. Y. Hwang, Y. Iwasa, M. Kawasaki, B. Keimer, N. Nagaosa, and Y. Tokura, Nat. Mater. **11**, 103 (2012).
[8] S.-W. Cheong, Nat. Mater. **6**, 927 (2007).
[9] M. D. McCluskey and E. E. Haller, *Dopants and Defects in Semiconductors* (CRC, Boca Raton, FL, 2012).
[10] C. Ton-That, L. Weston, and M. R. Phillips, Phys. Rev. B **86**, 115205 (2012).
[11] J. N. Eckstein, Nat. Mater. **6**, 473 (2007).
[12] C. G. Van de Walle, Phys. Status Solidi B **235**, 89 (2003).
[13] C. Tang, X. Lu, F. Huang, X. Wu, W. Cai, and J. Zhu, J. Appl. Phys. **105**, 061632 (2009).
[14] E. Ertekin, V. Srinivasan, J. Ravichandran, P. B. Rossen, W. Siemons, A. Majumdar, R. Ramesh, and J. C. Grossman, Phys. Rev. B **85**, 195460 (2012).
[15] P. G. Sundell, M. E. Björketun, and G. Wahnström, Phys. Rev. B **73**, 104112 (2006).
[16] D. J. Keeble, S. Wicklein, R. Dittmann, L. Ravelli, R. A. Mackie, and W. Egger, Phys. Rev. Lett. **105**, 226102 (2010).
[17] V. Jary, P. Bohacek, R. Mihokova, L. Havlak, B. Trunda, and M. Nikl, Opt. Mater. **35**, 1019 (2013).
[18] C. Van de Walle and J. Neugebauer, Nature (London) **423**, 626 (2003).
[19] J. T-Thienprasert, I. Fongkaew, D. J. Singh, M.-H. Du, and S. Limpijumnong, Phys. Rev. B **85**, 125205 (2012).
[20] P. G. Sundell, M. E. Björketun, and G. Wahnström, Phys. Rev. B **76**, 094301 (2007).
[21] M. E. Bjorketun, P. G. Sundell, and G. Wahnstrom, Faraday Discuss. **134**, 247 (2007).
[22] A. Janotti and C. G. Van de Walle, Nat. Mater. **6**, 44 (2007).
[23] J. Heyd, G. Scuseria, and M. Ernzerhof, J. Chem. Phys. **118**, 8207 (2003).
[24] M. Marsman, J. Paier, A. Stroppa, and G. Kresse, J. Phys.: Condens. Matter **20**, 064201 (2008).
[25] A. Janotti and C. G. Van de Walle, Phys. Status Solidi B **248**, 799 (2011).
[26] H.-P. Komsa and A. Pasquarello, Phys. Rev. B **84**, 075207 (2011).
[27] B. J. Kennedy, C. J. Howard, and B. C. Chakoumakos, Phys. Rev. B **59**, 4023 (1999).
[28] R. Schafranek, J. D. Baniecki, M. Ishii, Y. Kotaka, K. Yamanka, and K. Kurihara, J. Phys. D: Appl. Phys. **45**, 055303 (2012).
[29] J. Heyd, G. E. Scuseria, and M. Ernzerhof, J. Chem. Phys. **124**, 219906 (2006).
[30] J. P. Perdew, K. Burke, and M. Ernzerhof, Phys. Rev. Lett. **77**, 3865 (1996).
[31] A. V. Krukau, O. A. Vydrov, A. F. Izmaylov, and G. E. Scuseria, J. Chem. Phys. **125**, 224106 (2006).
[32] J. Perdew, M. Emzerhof, and K. Burke, J. Chem. Phys. **105**, 9982 (1996).
[33] P. E. Blöchl, Phys. Rev. B **50**, 17953 (1994).
[34] G. Kresse and J. Furthmüller, Phys. Rev. B **54**, 11169 (1996).
[35] C. G. Van de Walle and J. Neugebauer, J. Appl. Phys. **95**, 3851 (2004).
[36] C. Freysoldt, J. Neugebauer, and C. G. Van de Walle, Phys. Rev. Lett. **102**, 016402 (2009).

[37] C. Freysoldt, J. Neugebauer, and C. G. Van de Walle, Phys. Status Solidi B **248**, 1067 (2011).
[38] R. Evarestov, A. Bandura, V. Alexandrov, and E. Kotomin, Phys. Status Solidi B **242**, R11 (2005).
[39] J. R. Sambrano, V. M. Longo, E. Longo, and C. A. Taft, J. Mol. Struct. Theochem **813**, 49 (2007).
[40] A. Zhang, M. Lu, S. Wang, G. Zhou, S. Wang, and Y. Zhou, J. Alloys Compd. **433**, L7 (2007).
[41] Y. S. Lee, J. S. Lee, T. W. Noh, D. Y. Byun, K. S. Yoo, K. Yamaura, and E. Takayama-Muromachi, Phys. Rev. B **67**, 113101 (2003).
[42] R. Vali, Solid State Commun. **145**, 497 (2008).
[43] E. Mete, R. Shaltaf, and S. Ellialtioglu, Phys. Rev. B **68**, 035119 (2003).
[44] N. Sata, H. Matsuta, Y. Akiyama, Y. Chiba, S. Shin, and M. Ishigame, Solid State Ionics **97**, 437 (1997).
[45] M. W. Chase, C. A. Davies, J. R. Downey, D. J. Frurip, R. A. McDonald, and A. N. Syverud, J. Phys. Chem. Ref. Data **14**, 1 (1985).
[46] K. Xiong, J. Robertson, and S. J. Clark, J. Appl. Phys. **102**, 083710 (2007).